Physica C 494 (2013) 102–105

Contents lists available at SciVerse ScienceDirect

Physica C

journal homepage: www.elsevier.com/locate/physc

Material composition – Pinning strength correlation in Nb thin films with focused ion beam-milled washboard nanostructures

Oleksandr V. Dobrovolskiy [a,b,*], Evgeniya Begun [a], Michael Huth [a], Valerij A. Shklovskij [b,c]

[a] Physikalisches Institut, Goethe-Universität, 60438 Frankfurt am Main, Germany
[b] Physical Department, Kharkiv National University, 61077 Kharkiv, Ukraine
[c] Institute for Theoretical Physics, NSC-KIPT, 61108 Kharkiv, Ukraine

ARTICLE INFO

Article history:
Received 4 January 2013
Received in revised form 4 February 2013
Accepted 19 March 2013
Available online 29 March 2013

Keywords:
Superconducting Nb films
Washboard pinning potential
Focused ion beam milling
X-ray spectroscopy

ABSTRACT

An analysis of the interrelated changes in the material composition and the pinning strength in nanostructured Nb (1 1 0) thin films is presented. The nanopatterns were prepared by focused ion beam milling of an array of uniaxial grooves. They induce a washboard-like pinning potential landscape for vortices in the mixed state. By applying different magnetic fields, the most likely pinning sites along which the flux lines move through the samples have been selected. By this, either the background isotropic pinning of the pristine film or the enhanced isotropic pinning originating from the nanoprocessing has been probed. The enhanced pinning strength in the processed films has been found to correlate with the content of Ga implanted into the films during the nanopatterning.

1. Introduction

Within the last decade, nanostructured superconductors have received much attention because of associated technological and scientific reasons [1]. They provide direct access to the manipulation of Abrikosov vortices, or fluxons, with the help of tailored pinning potentials. This is due to the fact that fluxons, which are very sensitive to the alterations of the superconducting order parameter [2], represent a very useful tool for probing pinning and, thus, the degree of structural disorder associated with it in different parts of a nanostructured superconductor. An accurate adjustment of the fluxon dynamics is achieved by fine tuning the magnetic field. Accordingly, in this work, we have used three different magnetic fields for selectable probing most likely pinning sites along which the flux lines move through the patterned films. The motivation of our research is addressed next.

Superconductor Nb thin films with washboard-like nanopatterns provide a most accurate model system with fully predictable properties within a state-of-the-art theoretical approach [3]. This approach exactly describes the two-dimensional nonlinear vortex dynamics under competing anisotropic and isotopic pinning conditions in the single-vortex approximation. Whereas the existing works chiefly use lithographic techniques for the nanopatterning, we have decided to use a direct nanofabrication tool, focused ion beam (FIB) milling, taking advantage of high-quality periodic pinning profiles fabricated by using this technique (see Fig. 1a).

To our knowledge, the fabrication of pinning landscapes by FIB has been used in few works [4] so far. From literature it is known [5,6] that the gallium ions cause amorphization, implantation, and vacancy generation in the near-surface area of the processed region. However, a detailed study of the interrelated changes in the structural, magneto-transport, and pinning properties of FIB-patterned films has not been performed up to now. In the theory [3] the pinning strength is characterized by the depth of the pinning potential, its width, and its period length. Therefore, the estimation of the pinning potential depth U_0 for FIB-patterned samples is necessary for any reliable quantitative comparison of magneto-resistivity data with the theory [3,7,8]. Recently, we have performed a multifaceted study [9] of the influence of the direct nanoprocessing by FIB on the material composition, magneto-transport and pinning properties of epitaxial Nb (1 1 0) films via electrical dc transport measurements. In this early communication we report on a correlation of the pinning strength and the material composition in the FIB-patterned Nb films. We show that the pinning enhancement in the nanopatterned Nb films directly relates to the increasing content of Ga implanted into the films during the nanoprocessing. A detailed treatment of the magneto-resistivity data will be reported elsewhere [9].

2. Experimental

The samples are two nominally identical epitaxial Nb (1 1 0) films with a thickness of 52 nm. The films have been prepared in

* Corresponding author. Address: Physikalisches Institut Goethe-Universität, Frankfurt Max-von-Laue-Str. 1, 60438 Frankfurt am Main, Germany. Tel.: +49 69 798 47263; fax: +49 69 798 47291.
E-mail address: Dobrovolskiy@Physik.uni-frankfurt.de (O.V. Dobrovolskiy).

0921-4534/$ - see front matter © 2013 Elsevier B.V. All rights reserved.
http://dx.doi.org/10.1016/j.physc.2013.03.005

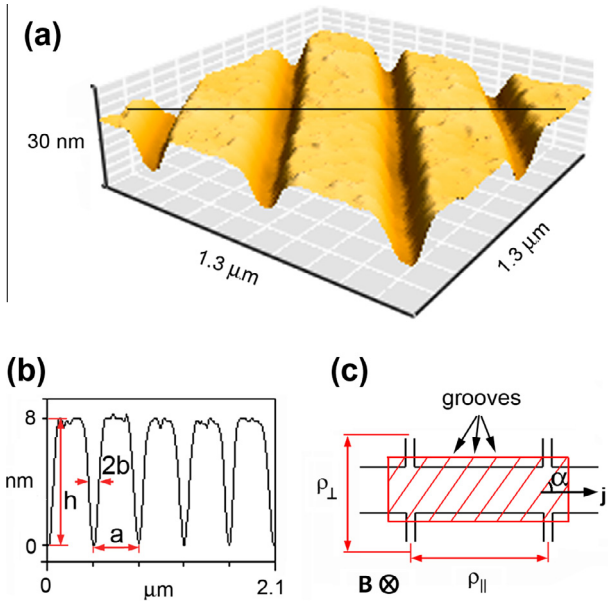

Fig. 1. Sample configuration in the general case. (a) Atomic force microscope image of the film surface taken in non-contact mode after the nanopatterning by FIB. The films were nanostructured with the pinning profile tilted at an angle α with regard to the **j**-direction. (b) Cross-section scan with the pinning nanoprofile parameters deduced along the black line in AFM image. The symbols $a = 420 \pm 2$ nm, $h = 8 \pm 0.5$ nm, and $2b = 60 \pm 3$ nm denote the average pinning potential period, depth, and the full width at half depth of a groove, respectively. (c) The experimental geometry: the Nb film with a thickness of 52 nm is placed into a small perpendicular magnetic field. A small transport current density **j** is applied to the sample. Experimentally deducible values are the longitudinal $\rho_{\parallel}$ and the transverse $\rho_{\perp}$ magneto-resistivities, determined relative to the direction of **j**.

parallel in the same deposition process by dc magnetron sputtering onto (1120) sapphire substrates. During the deposition process the substrates were kept at $T_s = 850$ °C, the Ar pressure was $p_s = 4 \times 10^3$ mbar, and the growth rate was $g = 1$ nm/s. Further details of the sample preparation and their structural characterization can be found in [10]. Both films were pre-patterned by standard photolithography followed by Ar ion-beam etching in order to define eight 4-contact 30×100 μm^2 bridge structures. In the following, each structure will be referred to as a sample. One sample has been left unpatterned for reference purposes, seven others have been nanostructured. Whereas the predefined 420 nm-periodic pinning profile (see Fig. 1b) was one and the same for all samples, its tilt angles with regard to the long strip of the bridge are $\alpha = 0°$,15°,30°,45°,60°, 75°, and 90°.

The nanopatterning was performed by FIB in a high-resolution scanning electron microscope (SEM, FEI Nova NanoLab 600). For the patterning process the beam parameters were 30 kV/30 pA in normal incidence and the dwell time was 1 μs. Calculations using Monte Carlo simulations [5] indicate that an implantation of Ga ions with such beam parameters occurs chiefly in a depth of up to 12 nm of the Nb film in the present case. The stopping of the Ga ions in the Nb film was simulated with the help of SRIM software. The average groove depth was pre-determined as 8 nm. It was deduced from *in situ* recorded changes in the electrical resistance of an additional 52 nm-thick Nb film during the FIB patterning.

Without exposure of the samples to air, an inspection using energy-dispersive X-ray spectroscopy (EDX) has been performed in the SEM right after the nanostructuring. The EDX parameters were 5 kV and 1.6 nA. Here the beam energy determines the effective thickness of the layer being analyzed, which is approximately 45 nm as calculated by the simulation program Casino. This corresponds to approximately 90% of the electron beam energy dissipated in the film. The material composition was calculated taking into account atomic number, absorption, fluorescence, and background corrections. The statistical error in elemental composition is 1.5%. The results are presented in Fig. 2. All spectra are normalized in such a way that the sum of the content of Ga and Nb in the sample is 100 at.%.

Transport measurements were carried out in a ^{4}He cryostat equipped with a superconducting solenoid. A small transport current density of $j = 6.4$ kA/cm^2 and fields $+\mathbf{B}$ and $-\mathbf{B}$ directed perpendicular to the film surface have been used. The experimental geometry is shown in Fig. 1c. The even longitudinal magneto-resistivity component was calculated according to the relation $\rho_{\parallel}^{+} = [\rho_{\parallel}(+\mathbf{B}) + \rho_{\parallel}(-\mathbf{B})]/2$.

3. Results and discussion

We begin our discussion with a comparison of the EDX spectra in Fig. 2. All the FIB-patterned structures show Ga apart from the dominating Nb peak. We note that the test area taken over 1 μm^2 in the patterned sample includes two grooves and the area close by. Thus, the content of 5.5 at.% can be considered as the average content of Ga in the nanostructure. To answer the question if there is any variation in the content of Ga in different regions of the pattern, the in-groove area and the area between the grooves have been probed. The in-groove spectrum reveals 11.5 at.% of Ga. At the same time, 2.5 at.% of Ga is found in the patterned structure away from the grooves. This must be caused by secondary and high-order collisions of Ga ions with Nb atoms. By this way, the EDX analysis clearly indicates that the material composition in the patterned structures is changed with respect to that of the as-grown film.

We proceed to the presentation of the superconducting properties of the samples. All nanostructured samples are superconducting below a critical temperature of $T_c = 8.61$ K which is slightly reduced with regard to that of the as-grown film for which it is 8.88 K. The critical temperature is determined as the temperature at which the resistivity has dropped to 90% of its extrapolated normal state value ρ_n. The spread in T_c for different nanostructured bridges is less than 5 mK. All patterned structures demonstrate a sharp superconducting transition with a width ΔT smaller than 0.05 K. These are broader than $\Delta T \approx 0.02$ K for the unpatterned sample. The temperature dependence of the upper critical field

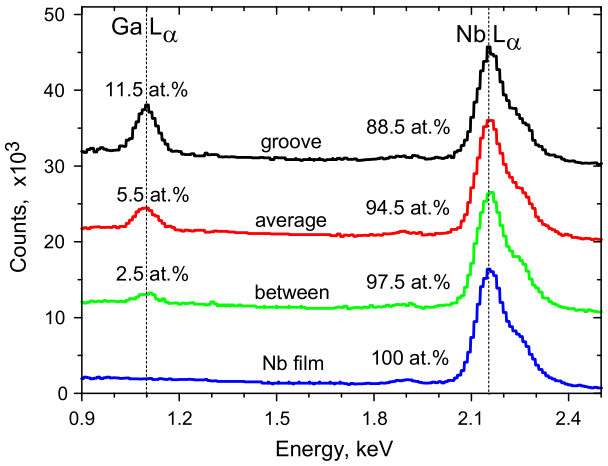

Fig. 2. Material composition in the as-grown Nb film and the same film after the nanopatterning (probed area 1×1 μm^2), as well as between the grooves and in the groove area (probed area 100×100 nm^2) revealed by EDX spectroscopy. Along the vertical axis, an offset of 10^3 counts is used to facilitate comparison. The peaks of Ga and Nb are indicated by vertical dashed lines.

$B_{c2}(T)$ can be well fitted by the standard expression $B_{c2}(T) = B_{c2}(0)[1-(T/T_c)^2]$ with the zero-temperature values $B_{c2}(0)$ for the non-patterned and the patterned samples as 1.55 T and 1.9 T, respectively.

We have measured the critical current j_c for the different α by using a 0.1 μV voltage criterium. The resulting polar plot of $j_c(\alpha)$ is shown in Fig. 3 for three selected magnetic fields B of 8.8, 11.7, and 15 mT, much less than the upper critical field $B_{c2}(T_j)$. Assuming a triangular vortex lattice these values are selected in such a way that the vortices are made to arrange in different configurations with respect to the underlying 420 nm-periodic pinning landscape. The field of 8.8 mT corresponds to the fundamental matching field, i.e., when all vortices are pinned at the groove bottoms and there are no interstitial vortices. The field of 11.7 mT represents the secondary matching field at which half the total number of vortices are pinned at the groove bottoms and the remaining vortices are pinned by randomly distributed isotropic pins in between. Finally, a field of 15 mT is selected as representative for a mismatching field, i.e., when a major fraction of vortices is interstitial. From Fig. 3 it follows that the difference $j_c(0°)/j_c(90°) \approx 2.1$ is most pronounced for the fundamental matching field of 8.8 mT. This ratio is reduced with increasing portion of vortices pinned between the grooves (see the curves for 11.7 and 15 mT). It should be noted that the overall shape of the curve $j_c(\alpha)$ for 8.8 mT is in good agreement with the theoretical predictions (see Fig. 18 in Ref. [3]).

Finally, we turn to an analysis of the temperature dependences of the magneto-resistive response for $\alpha = 0°$ and $\alpha = 90°$ in the patterned samples. See the main graph in Fig. 4. The behavior of $\rho_{\parallel}^{+}(T)$ for different α and B values differs substantially. The smoothed step-like $\rho_{\parallel}^{+}(T)$ curves are clearly anisotropic and their shape strongly depends on the angle α. Intermediate angles will be discussed in Ref. [9]. At 8.8 mT for $\alpha = 90°$, when all vortices move along the grooves, they are influenced only by the isotropic pinning at the groove bottoms. The isotropic pinning at the groove bottoms is much weaker that the anisotropic pinning and this is why a non-zero resistance "tail" is observed. On the contrary, when $\alpha = 0°$ the grooves effectively pin the vortices and the non-dissipative state is preserved up to higher temperatures. With increasing temperature the vortices finally are thermally activated from the grooves and the resistive transition in this case is most sharp. With increasing magnetic field, the step-like transitions become smoother as an increasing portion of vortices moves between the grooves where the isotropic pinning is weaker than at the groove bottoms. In order to quantify the pinning potential parameters, an Arrhenius analysis [11] of $\rho_{\parallel}^{+}(T)$ has been performed. For the fields 11.7 and 15 mT the appropriate portions of vortices pinned at the groove bottoms and between the grooves have been taken into account [9]. From the slopes of the Arrhenius plots the pinning activation energy has been calculated. The results appear in the inset in Fig. 4. From the deduced activation energies U_{eff} the depth of the isotropic pinning potential at the groove bottoms is $U_{0i} \approx 1000$ K and between the grooves it is $U_{0i} \approx 850$ K. These values are slightly increased with respect to the background isotropic pinning in the non-patterned film where $U_{0i} \approx 750$ K. It should be noted that the activation energy, i.e. strength of the anisotropic pinning for the vortex motion across the grooves is significantly higher, $U_{0a} \approx 6010$ K. The calculated depths of the pinning potential in the different areas of the FIB-patterned film are summarized in Fig. 5.

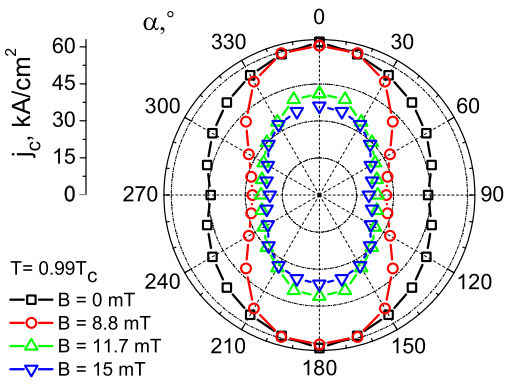

Fig. 3. Polar plot of the critical current density $j_c(\alpha)$ at $T = 0.99T_c$ for a set of fields, as indicated. The $j_c(\alpha)$ curves are obtained by replicating on all quadrants the original data of the first quadrant.

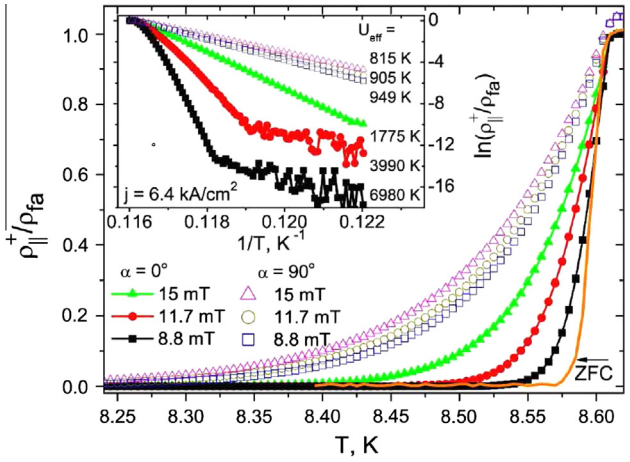

Fig. 4. Main graph: The temperature dependence of the even longitudinal magneto-resistivity component $\rho_{\parallel}^{+}(T)$ for the grooves orientations $\alpha = 0°$ and $\alpha = 90°$. All curves are normalized by the flux-flow resistivity $\rho_{fa} = \rho_n B_a / B_{c2}(T)$, where $B_a = 8.8$ mT. Inset: The corresponding Arrhenius plots with the deduced activation energies U_{eff} labeled close to the curves. The zero-field cooling (ZFC) curve for $\alpha = 0°$ normalized by the normal-state resistivity ρ_n is shown for comparison. See text for details.

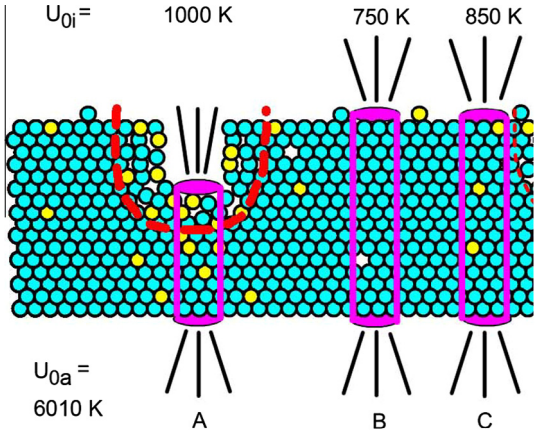

Fig. 5. Out-of-scale representation of the changes in the structural and the associated pinning properties of the films invoked by FIB milling. Blue circles correspond to Nb atoms, yellow ones to Ga implants from the FIB, and the background point-like disorder is shown by empty spaces. The dashed line marks the amorphous area. Solid cylinders illustrate fluxons pinned by different parts of the sample: Vortex A is pinned by a groove which acts as a strong anisotropic pin with a high activation energy $U_{0a} \approx 6010$ K for $\alpha \approx 0°$. When $\alpha = 90°$, for the vortex motion along the groove bottom the isotropic pinning is slightly increased ($U_{0i} \approx 1000$ K, vortex A) with respect to its value in the unpatterned film ($U_{0i} \approx 750$ K, vortex B) and between the grooves ($U_{0i} \approx 850$ K, vortex C). (For interpretation of the references to color in this figure legend, the reader is referred to the web version of this article.)

Let us compare the calculated pinning parameters with the values known from literature. For instance, the activation energy for the vortex motion across twinning planes in high-temperature superconductors is of the order of 1000 K [12]. In Nb films grown by molecular beam epitaxy on facetted sapphire substrates this value is between 1600 and 4000 K [11]. Accordingly, in the present experiment from the activation energies it appears that the fabricated grooves act as very strong anisotropic pins. At the same time, background isotropic pinning is revealed to be weaker than that in Ref. [11]. A possible reason for this is that in the present work the films are a factor of 2 thicker and thus, the thickness-induced suppression of the superconducting order parameter must be smaller. The strength of the anisotropic pinning invoked by the grooves can be attributed to the following factors. First, the reduction of the length of a vortex being pinned by a groove renders pinning to be more effective there due to vortex energy reduction. Second, Ga implants stopped in the sample underneath the milled groove provide strong pins. Third, additional sources of pinning are provided by the amorphization of and the vacancy generation in Nb caused by the Ga ion bombardment. Finally, the superconducting order parameter is suppressed due to the reduced film thickness at the position of the grooves. All these mechanisms have the same effect and cause a rather strong anisotropic pinning potential which makes the anisotropic effects clearly visible.

4. Conclusion

Summarizing, the employed nanoprocessing has been revealed to change the material composition and the pinning properties of the FIB-patterned films. The most pronounced local pinning enhancement has been found at the groove bottoms, i.e. the areas subjected to a most intensive bombardment by the Ga atoms during the FIB-patterning. The pinning anisotropy in the mixed state has been revealed to be most pronounced for the fundamental matching field of 8.8 mT when all vortices are pinned at the groove bottoms. The reported features enable a forthcoming comparison of the experimental data with a state-of-the-art theoretical approach [3] describing the two-dimensional nonlinear vortex dynamics under competing anisotropic and isotopic pinning conditions.

Acknowledgements

OVD gratefully acknowledges financial support by the DFG through Grant No. DO 1511/2-1. EB thanks the Beilstein-Institut, Frankfurt/Main, Germany, for financial support within the research collaboration NanoBiC.

References

[1] A.V. Silhanek, J. Van de Vondel, V.V. Moshchalkov, Guided Vortex Motion and Vortex Ratchets in Nanostructured Superconductors, Springer-Verlag, Berlin Heidelberg, pp. 1–24.
[2] E.H. Brandt, The flux-line lattice in superconductors, Rep. Progr. Phys. 58 (1995) 1465–1594.
[3] V.A. Shklovskij, O.V. Dobrovolskiy, Influence of pointlike disorder on the guiding of vortices and the Hall effect in a washboard planar pinning potential, Phys. Rev. B 74 (2006) 104511–1–14.
[4] A. Pautrat, J. Scola, C. Goupil, C. Simon, C. Villard, B. Domengès, Y. Simon, C. Guilpin, L. Méchin, Quantitative analysis of the critical current due to vortex pinning by surface corrugation, Phys. Rev. B 69 (2004) 224504–1–5.
[5] J.F. Ziegler, J.B. Biersack, U. Littmarck, The Stopping and Ranges of Ions in Solids, Pergamon, New York, 1985.
[6] I. Utke, P. Hoffmann, J. Melngailis, Gas-assisted focused electron beam and ion beam processing and fabrication, J. Vac. Sci. Technol. B 26 (2008) 1197–1276.
[7] V.A. Shklovskij, O.V. Dobrovolskiy, AC-driven vortices and the Hall effect in a superconductor with a tilted washboard pinning potential, Phys. Rev. B 78 (2008) 104526–1–12.
[8] V.A. Shklovskij, O.V. Dobrovolskiy, Frequency-dependent ratchet effect in superconducting films with a tilted washboard pinning potential, Phys. Rev. B 84 (2011) 054515–1–12.
[9] O.V. Dobrovolskiy, E. Begun, M. Huth, and V.A. Shklovskij. Electrical transport and pinning properties of Nb thin films patterned with focused ion beam-milled washboard nanostructures. New J. Phys. 14 (2012) 113027–1–27.
[10] O.V. Dobrovolskiy, M. Huth, Crossover from dirty to clean superconducting limit in dc magnetron-sputtered thin Nb films, Thin Solid Films 520 (2012) 5985–5990.
[11] O.K. Soroka, V.A. Shklovskij, M. Huth, Guiding of vortices under competing isotropic and anisotropic pinning conditions: theory and experiment, Phys. Rev. B 76 (2007) 014504-1–014504-12.
[12] T.T.M. Palstra, B. Batlogg, L.F. Schneemeyer, J.V. Waszczak, Thermally activated dissipation in BiSrCaCuO, Phys. Rev. Lett. 61 (1988) 1662–1665.